(Received 4 March 2026, Accepted 15 April 2026, Scheduled 25 April 2026)

Compact 13.56 MHz Wireless Power Transfer Architecture Using Self-Resonant Coils with Inherent Source Power Limiting

Zixuan Yi, Ziheng Li, Xiaojun Tao, and Meiling Li*

Key Laboratory of Specialty Fiber Optics and Optical Access Networks
Shanghai Institute of Advanced Communication and Data Science, Shanghai University, Shanghai, China

ABSTRACT: Megahertz wireless power transfer (MHz-WPT) enables compact resonant components; yet the matching, compensation, and filtering stages used in conventional systems can dominate loss and standby dissipation at MHz operation. To address this issue, this work proposes a compact 13.56 MHz WPT architecture in which impedance transformation is integrated into the resonant hardware. A self-resonant transmitting coil is co-designed with a Class-E power amplifier to shape the reflected load toward the optimum operating condition, thereby removing the external compensation network, additional matching stage, and lumped-element LC output filter. The analysis shows that, when the receiver is removed, the effective load becomes dominated by the transmitter resistance, inherently suppressing delivered power without sensing or closed-loop control. A prototype delivers 9 W over 30 mm with 81.5% end-to-end DC-DC efficiency, while under receiver absence, the DC input power decreases from 11 W to 1.15 W. These results demonstrate a simplified and robust MHz-WPT architecture with reduced component count and inherently low standby dissipation.

1. INTRODUCTION

Wireless power transfer (WPT) is being actively pursued for mobile electronics, smart terminals, and electric vehicles, where frequent charging and user convenience are paramount [1–3, 20]. Moving WPT into the MHz band offers smaller resonant components and greater placement flexibility than conventional hundreds-of-kilohertz systems [4–-6] as shown in Fig. 1. Yet, at these higher frequencies, the supporting hardware that is often secondary at kHz — matching/compensation networks, gate driving and control interfaces — can become a first-order loss and volume contributor because component quality factors degrade, and parasitic effects are no longer negligible [7–11]. The result is a tangible penalty in end-to-end DC-DC efficiency and standby consumption.

Another key challenge is robust operation under intermittent coupling. In practical use, the receiver may repeatedly approach, misalign, or depart from the transmitter. For commonly used compensated links, receiver removal can shift the power stage away from its intended operating point, causing increased device stress, degraded soft switching, and potential safety concerns unless additional protection or feedback is introduced [12, 13, 19]. Recent MHz-WPT studies have improved robustness mainly through regulation-oriented approaches, such as frequency/duty control, wide-range operation, and wireless phase-shift regulation [27–30]. In parallel, self-resonant and resonance-integrated coils have been explored to reduce discrete compensation components and improve compactness [14, 17, 24, 31, 32]. Nevertheless, the former route mainly emphasizes regulation, whereas the latter mainly focuses on coil or resonator design itself.

Motivated by these limitations, this paper targets a compact MHz WPT system that is both hardware-minimal and inherently safe under receiver absence. The key idea is to embed resonance and impedance shaping into self-resonant antisymmetric planar coils (APCs), thereby eliminating standalone compensation capacitors and external matching networks [14–18]. We then co-design a Class-E power amplifier with the transmitting APC so that the coil serves as the resonant filter and presents the optimal Class-E load under normal operation, while naturally collapsing the source power to a low level when the receiver is removed by making the transmitter coil resistance the effective load. A 13.56-MHz Industrial, Scientific, and Medical (ISM) implementation is presented to substantiate the approach.

2. PROPOSED MHz WPT SYSTEM

The proposed megahertz wireless power transfer (WPT) system has three functional blocks: a power source, a pair of coupling coils, and a rectifier [22]. As shown in Fig. 2(a), the coils provide magnetic coupling while also setting the resonant condition and transforming the load impedance. The source delivers the high-frequency drive, and the rectifier converts the received AC power to DC for the load. By removing the matching and compensation networks, as well as any dedicated control module, the system becomes more compact and can operate at higher efficiency.

To directly support the claim of reduced component count and simplified architecture, Table 1 compares the proposed system with a conventional compensated MHz-WPT architecture at the functional-block level. Unlike the conventional chain, which typically consists of a power source, a matching network,

* Corresponding author: Meiling Li (meilingli@shu.edu.cn).

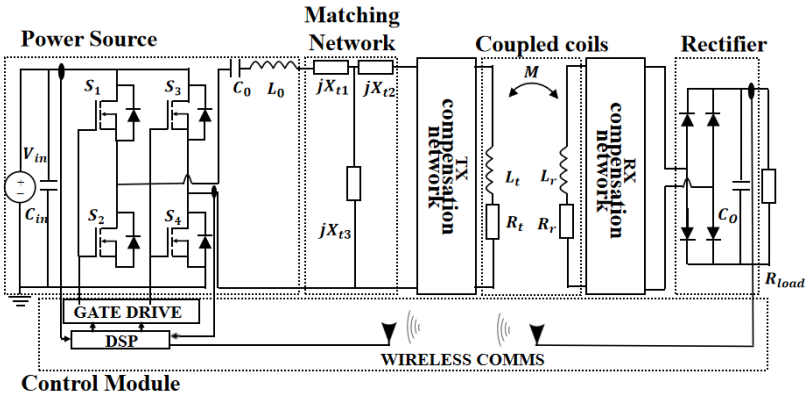

FIGURE 1. Equivalent circuit of a typical kHz WPT system.

TABLE 1. Quantitative comparison between a conventional compensated MHz-WPT architecture and the proposed architecture.

Aspect	Conventional	Proposed	Benefit
Functional blocks	6	3	Simpler architecture
Matching network	Required	Eliminated	Lower passive count
Compensation capacitors	Required	Eliminated	Lower passive loss
Source-side resonant tank	Separate L_0C_0	Absorbed into coils	Lower hardware burden
Protection/Control	Often required	Not Required	Inherent low-power behavior
Receiver-absence DC input power	Not architecture-limited	1.15 W	Lower standby dissipation

a compensation network, coupled coils, a rectifier, and a protection/control interface, the proposed system retains only three essential blocks: the power source, self-resonant coupled coils, and rectifier. In addition, the source-side resonant/filtering function is absorbed into the transmitting coil, and no dedicated sensing or closed-loop protection module is required for receiver absence.

2.1. Power Source

A single-switch switching-mode Class-E power amplifier (PA), operated as a DC-RF inverter, was adopted as the front-end power source (Fig. 2(b)). The PA was driven at ω_0 from a DC supply V_D through an RF choke L_f, with a parallel capacitance C_s to satisfy the Class-E switching conditions, and an output resonant network L_0C_0 that shapes the switching waveform and presents an appropriate load to the inverter. At the fundamental frequency ω_0, the series L_0C_0 output network was designed to present a net reactance jZ_{LC} to the Class-E stage and its quality factor as Q_0. Under the standard Class-E design relations, these quantities satisfied (1)–(5).

$$jZ_{LC} = \frac{V_{LC}}{I_O} = j\omega L_0 + \frac{1}{j\omega C_0} \tag{1}$$

$$C_0 = \frac{1}{\omega R Q_0} \tag{2}$$

where ω is the angular frequency. The relationship between R and Z_{LC} can be obtained by analyzing the load network [23]:

$$Z_{LC} = \frac{\pi R\left(\pi^2 - 4\right)}{16} \tag{3}$$

$$L_0 = \frac{RQ_0}{\omega} + \frac{\pi R\left(\pi^2 - 4\right)}{16\omega} = L_{01} + L_{02} \tag{4}$$

Equation (4) highlights that L_0 contains a term proportional to $L_{01} = RQ_0/\omega$ that sets the resonant loop quality factor, and $L_{02} = \pi R(\pi^2 - 4/(16\omega)$ provides the required excess inductive reactance for the Class-E switching condition. Accordingly, the design is constrained by

$$\omega_0 = \frac{1}{\sqrt{L_{01}C_0}}, \quad Z_{LC} = \omega_0 L_{02} \tag{5}$$

where L_{01} and C_0 represent the corresponding resonant-loop parameters of the Class-E output network defined in (1)–(4). Therefore, the transmitter-side equivalent resonant loop can satisfy the design requirement imposed on the Class-E output network.

This observation enables a compact realization: rather than implementing L_0C_0 as a dedicated discrete (or integrated) tank, the required resonant behavior can be embodied by the transmitter coil itself, provided that the coil exhibits sufficiently high Q around ω_0. In practice, this reduces the component count and associated loss and removes an otherwise separate resonant network from the power stage. Moreover, because the additional inductive term in (4) is small in our design, it can also be absorbed into the transmitter coil implementation, further simplifying the power source.

2.2. Coupling Coils

In conventional MHz WPT links, resonance is typically established by adding discrete compensation capacitors, which increases the component count and introduces additional loss and

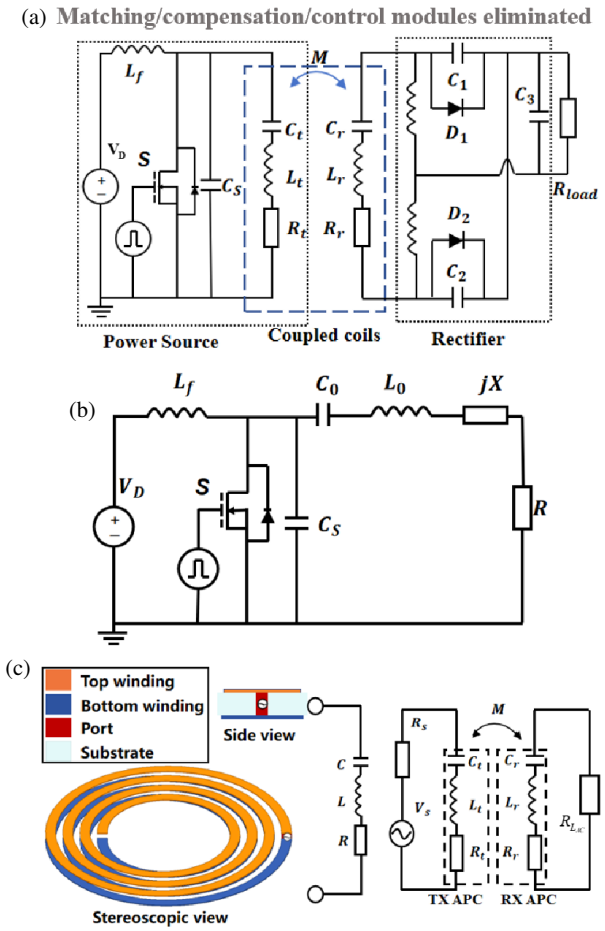

FIGURE 2. Equivalent circuit of (a) proposed system, (b) class-E power amplifier, (c) coupling coils.

volume. To embed the required capacitance within the coupling structure, we implement coupling coils as antisymmetric planar coils (APCs) [24]. The APC employs two spiral windings on opposite sides of a dielectric substrate, whose close spacing creates a large interlayer distributed capacitance. In addition to the coil inductance, this capacitance enables self-resonant behavior near the operating frequency, thereby reducing the need for discrete compensation capacitors.

At the fundamental frequency ω_0, the coupled coils can be modeled using an equivalent circuit with series parameters (R_t, L_t) and (R_r, L_r) for the transmitter (TX) and receiver (RX) coils, respectively, and mutual inductance M between them. The rectifier and DC load are represented by an equivalent AC resistance $R_{L,AC}$ connected at the RX side under the fundamental-harmonic approximation. On the source side, an AC excitation V_s is applied with a source resistance R_s (representing the source output resistance seen by the resonant link).

Because the proposed architecture does not employ a dedicated matching network, the impedance conditions required by the power stage must be satisfied through coil design. Following the two-port coupled-inductor analysis in [21], the load and source resistances that maximize the coil-to-coil power transfer efficiency satisfy:

$$R_{L_{AC}} = \sqrt{(R_t R_r + \omega^2 M^2) R_r / R_t} \tag{6}$$

$$R_S = \sqrt{(R_t R_r + \omega^2 M^2) R_t / R_r} \tag{7}$$

Under the high-efficiency condition $\omega^2 M^2 \gg R_t R_r$, (6)–(7) are reduced to the compact forms (8) and (9):

$$R_{L_{AC}} = \omega M \sqrt{\frac{R_r}{R_t}} = \omega M N_2^2 \sqrt{\frac{\rho_4 + \rho_3}{\rho_4 - \rho_3}} \tag{8}$$

$$R_s = \omega M \sqrt{\frac{R_t}{R_r}} = \omega M N_1^2 \sqrt{\frac{\rho_2 + \rho_1}{\rho_2 - \rho_1}} \tag{9}$$

$$\frac{R_S}{R_{L_{AC}}} = \frac{N_1^2}{N_2^2} \sqrt{\frac{\rho_2 + \rho_1}{\rho_2 - \rho_1}} \sqrt{\frac{\rho_4 - \rho_3}{\rho_4 + \rho_3}} \tag{10}$$

Here, N_1, ρ_1, and ρ_2 denote the number of turns, inner radius, and outer radius of the TX coil, respectively; N_2, ρ_3, and ρ_4 denote the same parameters for the RX coil. Once the desired optimal load level is specified (through $R_{L,AC}$), the source-side optimal resistance R_S can be matched by selecting the turn ratio N_1/N_2 and tuning the inner/outer radius of both coils. In this way, the geometric parameters of the APCs serve as effective design degrees of freedom to realize impedance matching without an additional matching network.

3. AUTOMATIC SOURCE POWER PROTECTION SCHEME

The removal of a receiver can push a WPT transmitter into an undesirable operating point, especially when the receiver status is not sensed at the transmitter. In conventional compensated links, the power stage may continue operating near its nominal condition under abnormal loading, which can increase switch stress and device temperature. A dedicated feedback control improves robustness; however, it also adds hardware complexity and cost.

In this section, design rules are derived for the proposed architecture to realize intrinsic source-side power reduction under receiver absence, without relying on additional sensing, communication, or control circuitry. The present work focuses on intrinsic source-power reduction under receiver absence rather than active load detection or closed-loop battery charging control.

Figure 3(a) shows the equivalent circuit used for the analysis. The DC input current is denoted by i_D, the switch drain current by i_s, and the shunt-capacitor current by i_c. The drain voltage is denoted by v_{ds} (labeled as V_s in Fig. 3(a)) and the output voltage by V_o. The losses in the output path are lumped into an equivalent resistance R_L, while the remaining modules connected after the power amplifier are represented by an equivalent load term.

The Class-E stage, therefore, sees an effective loading R_p. To keep the following derivation consistent with the coupled-coil model in Section 2.2, the downstream WPT link is analyzed through its tuned series-series (SS-equivalent) branch at the fundamental frequency ω_0. Under the fundamental-harmonic approximation, the RX-side rectifier and DC load are represented by the equivalent AC resistance $R_{L,AC}$. Along the tuned operating branch relevant to the present prototype, the net reactance seen from the TX side vanishes at ω_0, so the reflected

(a) **Conventional architecture**

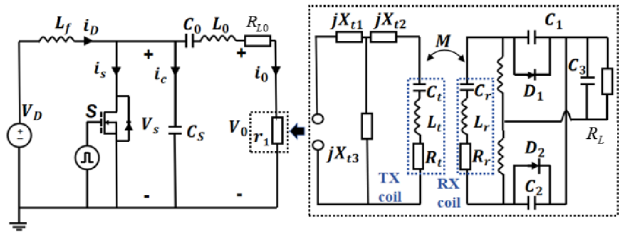

(b) **Proposed architecture**

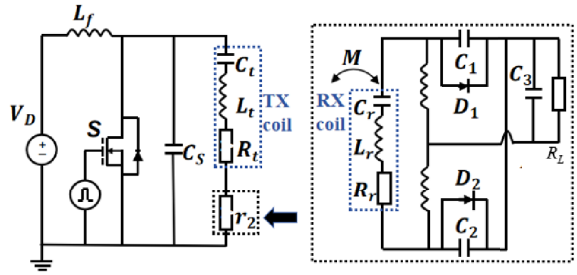

FIGURE 3. Equivalent circuit of (a) traditional WPT system modules connected after the Class-E power amplifier, (b) the remaining novel WPT architecture modules connected after the power source.

impedance is purely resistive. Therefore, the effective source-side load is

$$R_p = R_{L0} + r_1 \tag{11a}$$

$$R_p = R_t + \frac{\omega_0^2 M^2}{R_r + R_{L_{AC}}} \tag{11b}$$

When the receiver departs, $M \to 0$, and thus $R_p \to R_t$. Under the standard Class-E relations for $D = 0.5$ [25], the delivered power is a function of the effective load R_p. For compactness, let

$$K = 8\pi^2 \omega_0^2 C_s^2 V_D^2 \tag{12a}$$

$$A(\phi) = \pi \cos(\phi) - 2\sin(\phi) \tag{12b}$$

$$G(R_p, \phi) = \pi^3 \omega_0 C_s R_p + 8\sin^2\phi \tag{12c}$$

Then, the output power and the phase term can be written as

$$P_0(R_p, \phi) = K \frac{R_p A(\phi)}{G(R_p, \phi)^2} \tag{12d}$$

$$\phi(R_p) = \arctan\left(\frac{\frac{\pi^2}{2} - 4 - 2\pi\omega_0 C_s R_p}{\pi\left(1 + \pi\omega_0 C_s R_p\right)}\right) \tag{12e}$$

Since ϕ depends on R_p, the load sensitivity must be evaluated through the strict total derivative

$$\frac{dP_0}{dR_p} = \frac{\partial P_0}{\partial R_p} + \frac{\partial P_0}{\partial \phi}\phi'(R_p) \tag{13}$$

Therefore, the source power is load-dependent through R_p, and its sensitivity to receiver-side loading must be evaluated through the total derivative in (13). More importantly, for the tuned SS-equivalent operating branch,

$$M \to 0 \Rightarrow R_p \to R_t \tag{14a}$$

$$\lim_{R_p \to 0} P_0(R_p) = 0 \tag{14b}$$

Hence, when the receiver is removed and the coupling collapses, the effective source-side load is driven toward the small-R_p side, where the Class-E source naturally enters a low-power operating region.

In the proposed architecture, the dedicated matching network is removed, and the impedance conditions are satisfied through coil design. The remaining modules connected after the power source (Fig. 3(b)) can be summarized as follows:

$$R_{P2} = R_t + r_2 = R_t + \frac{\omega^2 M^2}{(R_r + R_{L_{AC}})} \tag{15}$$

Here, the term $r_2 = \omega^2 M^2/(R_r + R_{L,AC})$ represents the receiver-side reflected resistance seen from the TX side at the fundamental frequency. When the receiver departs, $M \to 0$ and thus $r_2 \to 0$, so $R_{P2} \to R_t$. As R_t is typically small compared with the designed full-load effective resistance, (14b) implies that the source naturally shifts toward a low-power condition without any external control action. This intrinsic behavior mitigates excessive thermal rise under receiver absence, as further supported by the measurements in the experimental verification section.

4. EXPERIMENTAL VERIFICATION AND PERFORMANCE EVALUATION

To validate the proposed 13.56-MHz architecture, a hardware prototype was built using a pair of antisymmetric planar coils (APCs) as the TX-RX coupler (Fig. 4). The coils were aligned face-to-face with a 30-mm separation. A GS61004B GaN MOSFET was used as a switching device. The DC supply was set to $V_D = 20$ V, and the power stage was designed to deliver 11 W at the operating frequency.

$$R_{\text{opt}} = \frac{8}{\pi^2 + 4} \cdot \frac{V_{\text{in}}^2}{P_{\text{out}}} \tag{16}$$

$$C_{s,total} = \frac{0.1836}{\omega R_{\text{opt}}} \tag{17}$$

The optimal source-side resistance required by the Class-E stage is estimated by (16), yielding $R_{\text{opt}} \approx 21.5\Omega$, which gives $C_{s,total} \approx 100.2$ pF, at 13.56 MHz. Since the implemented capacitor corresponds to the external shunt capacitor, the effective device output capacitance and layout parasitics are also taken into account, and the practical capacitor is selected as

$$C_s = C_{s,total} - C_{effc} - C_{layout} = 80.8\,\text{pF} \tag{18}$$

Following standard Class-E design practice, the RF-choke inductance L_f and shunt capacitor C_s were selected as 2 µH and 80.8 pF, respectively, which is used as a target for the subsequent coil and system design.

To ensure proper impedance matching between the power source and coupling coils, the load seen at the source terminals must equal the optimal source resistance indicated in Fig. 2(c). In the prototype, the rectifier uses DFLS1150 Schottky diodes

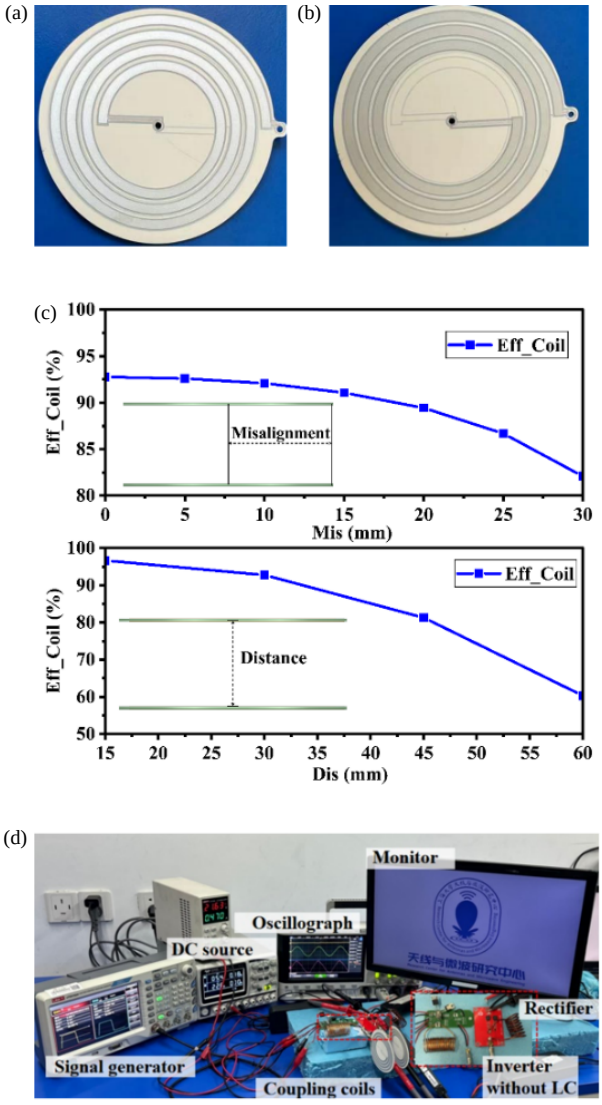

FIGURE 4. (a) Fabricated Tx APC. (b) Fabricated Rx APC. (c) Variation in coil efficiency under lateral misalignment and axial separation. (d) Experimental setup demonstrating 9 W DC output to a monitor at a 30 mm coil separation.

to reduce reverse-recovery loss at 13.56 MHz, and the practical end-use device is a monitor, whose equivalent AC load at the receiver side is 22.5 Ω. Therefore, the equivalent AC load in the circuit of Fig. 2(c) is designed to be 22.5 Ω so that the reflected impedance meets the Class-E optimum load condition. By substituting the target load values into (10), the geometries of the TX and RX coils — such as turn numbers and dimensions — are determined to satisfy the matching requirement. The resulting design parameters of the APC coils are summarized in Table 2.

The fabricated TX and RX coils are shown in Figs. 4(a)–(b). The coil parameters were extracted using a vector network analyzer (Keysight N5227A) after SOLT calibration. Electrical waveforms were measured by an oscilloscope (Keysight DSOX3024T) with voltage and current probes. The temperature comparison was performed at 26°C after 20 min of continuous operation for each case. AC-AC and DC-DC efficiencies were calculated from the measured terminal quantities, with the

TABLE 2. Parameter values of coupling coils.

Parameter	Value
Number of turns of TX coil	3.5
Number of turns of RX coil	3
Inductance of TX coil	1.33 μH
Capacitance of TX coil	145.1 pF
Resistance of TX coil	0.39 Ω
Quality factor of TX coil	207.4
Inner diameter of TX coil	17 mm
Outer diameter of TX coil	35 mm
Inner diameter of RX coil	25 mm
Outer diameter of RX coil	35 mm

main uncertainty sources being coil-parameter deviation, self-resonant-frequency shift, and ordinary instrument tolerances.

The simulation results of the offset operating point between coils are shown in Fig. 4(c), and the experimental setup is shown in Fig. 4(d). Under the nominal condition, the prototype delivers 9 W DC to the load with an 11 W DC input. Under the nominal operating condition, the coupling coefficient between the transmitting and receiving coils was calculated to be 0.18 using the filament-current method.

Waveform measurements were performed at the same operating point as Figs. 5(a)–(c). The TX-side current remains close to sinusoidal, indicating that the resonant link dominates the fundamental power transfer without an added discrete output filter between the inverter and the TX coil. The measured DC input and DC output quantities further confirm stable operation at the designed frequency.

AC-AC efficiency between the coils is calculated to be 93%, and end-to-end DC-DC efficiency is 81.5%. To evaluate the intrinsic protection behavior, the receiver was removed while keeping the supply voltage and operating frequency unchanged. In this case, the DC input power automatically drops to 1.15 W (about 10% of the full-load case). To probe tolerance sensitivity, the resonant frequency of the integrated network was perturbed by ±3% while the operating frequency was held at 13.56 MHz. The simulated efficiency varied by less than ±4%, suggesting that the proposed architecture is not unduly sensitive to modest detuning.

Figure 6 shows the power-stage temperature also stabilizes at a much lower level: after 20 minutes of continuous operation at an ambient temperature of 26°C, the measured temperature decreases from 105.2°C (under nominal full-load operation) to 53.7°C (receiver absent). These results support the intrinsic source-side power reduction predicted by the analysis above and confirm the practical effectiveness of the proposed architecture.

Table 3 summarizes a comparison between the proposed MHz WPT architecture and several representative MHz WPT systems reported in recent years. For example, in one reported system [26], a three-dimensional spiral coupling coil is adopted, which enables high AC-AC efficiency but still yields only moderate end-to-end DC system efficiency. Other MHz WPT systems employ various strategies to enhance efficiency and inte-

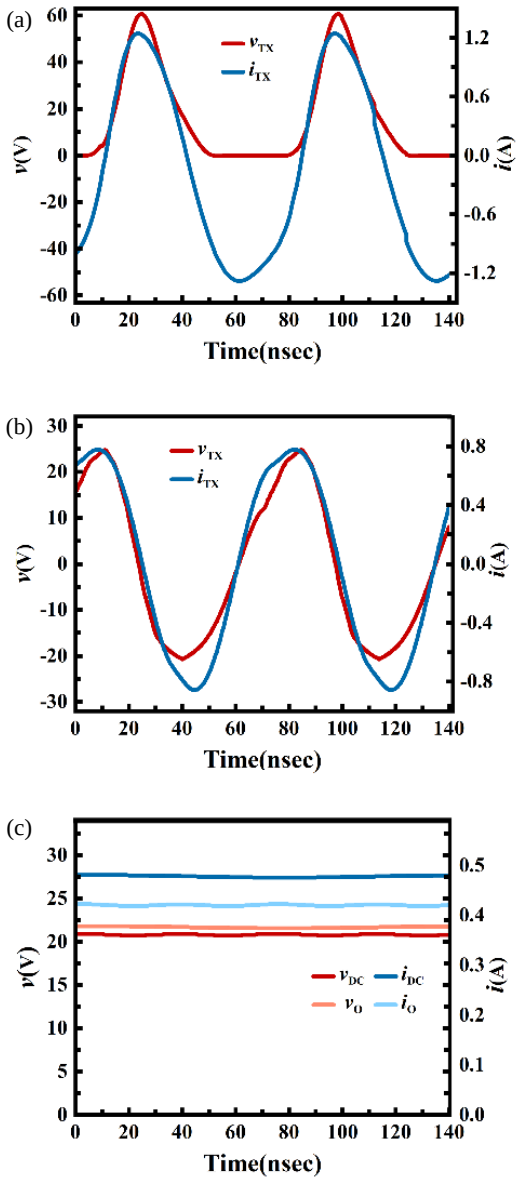

FIGURE 5. (a) Measured voltage and current at the TX coil terminals. (b) Measured voltage and current at the RX coil terminals. (c) Waveform measurements for DC input and output.

gration; yet their overall DC system efficiencies are still around 75%. Self-resonant coils have also been demonstrated with high AC-AC efficiency [14]; however, the coil and architecture developed in this work further improve the AC-AC performance while reducing component count. At 13.56 MHz, the proposed system achieves, to the best of our knowledge, one of the highest reported [27–29] DC-DC efficiencies in this power range while simultaneously resolving the inherent safety issue of SS compensated WPT systems when the receiver is absent.

5. CONCLUSION

This paper has presented a compact 13.56-MHz WPT architecture that reduces component count and improves safety by combining a Class-E power amplifier with self-resonant APC coils. In the proposed system, the transmitting coil simultaneously acts as a resonant filter, and the matching and compensation networks are eliminated. A circuit analysis has been carried out to clarify the relationship between the Class-E output power and the equivalent load seen at the source terminals. Based on this analysis, design guidelines have been derived so that the internal resistance of the transmitting coil becomes the dominant load when the receiver is removed, and the source power is inherently limited without any auxiliary control circuitry.

A 13.56-MHz prototype validates the concept. At a 30-mm transfer distance, the system delivers 9 W with 93% AC-AC efficiency and 81.5% end-to-end DC-DC efficiency. Upon receiver removal, the DC input power drops from 11 W to 1.15 W, and the power-stage temperature after 20 min decreases from 105.2°C to 53.7°C, supporting the proposed self-protection mechanism. This architecture is well suited for compact MHz WPT applications that require both high efficiency and safe operation under receiver absence.

TABLE 3. Comparison of reported MHz WPT architecture and proposed novel WPT architecture.

Ref.	f (MHz)	Diameter (mm)	d (mm)	η_{AC}	η_{DC}
[26]	13.56	70	500	90%	75%
[27]	13.56	30	1	N/A	65.9%
[28]	13.56	150	30	N/A	60%
[14]	6.78	50	30	80%	N/A
[29]	6.78	NA	30	81%	51%
This work	13.56	38	30	93%	81.5%

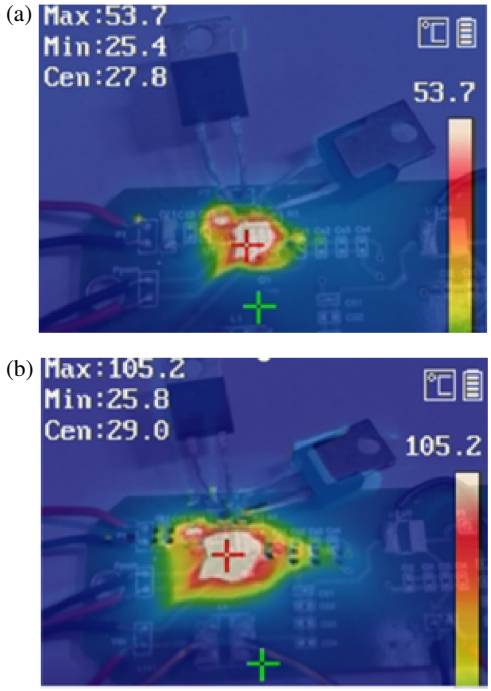

FIGURE 6. Temperature comparison of power source end after 20 minutes of operation. (a) Only transmitting end (receiving end left) vs. (b) Normal system operation (thermally stressed full-load condition).

ACKNOWLEDGEMENT

This work is supported in part by the National Natural Science Foundation of China under 52207214.

REFERENCES

[1] Fereshtian, A. and J. Ghalibafan, "Impedance matching and efficiency improvement of a dual-band wireless power transfer system using variable inductance and coupling method," *AEU — International Journal of Electronics and Communications*, Vol. 116, 153085, 2020.

[2] Hojjati-Firoozabadi, A., A. Azarfar, and M. Shahabadi, "Compact wireless power transfer system with microstrip-driven coupled dielectric resonators," *AEU — International Journal of Electronics and Communications*, Vol. 127, 153445, 2020.

[3] Kim, H.-J., H. Hirayama, S. Kim, K. J. Han, R. Zhang, and J.-W. Choi, "Review of near-field wireless power and communication for biomedical applications," *IEEE Access*, Vol. 5, 21 264–21 285, Sep. 2017.

[4] Tang, S. C., F. A. Jolesz, and G. T. Clement, "A wireless batteryless deep-seated implantable ultrasonic pulser-receiver powered by magnetic coupling," *IEEE Transactions on Ultrasonics, Ferroelectrics, and Frequency Control*, Vol. 58, No. 6, 1211–1221, Jun. 2011.

[5] Li, X., C. Wang, H. Wang, X. Dai, Y. Sun, and A. P. Hu, "A robust wireless power transfer system with self-alignment capability and controllable output current for automatic-guided vehicles," *IEEE Transactions on Power Electronics*, Vol. 38, No. 10, 11 898–11 906, Oct. 2023.

[6] Zhu, J.-Q., Y.-L. Ban, Y. Zhang, Z. Yan, R.-M. Xu, and C. C. Mi, "Three-coil wireless charging system for metal-cover smartphone applications," *IEEE Transactions on Power Electronics*, Vol. 35, No. 5, 4847–4858, May 2020.

[7] Li, S. and C. C. Mi, "Wireless power transfer for electric vehicle applications," *IEEE Journal of Emerging and Selected Topics in Power Electronics*, Vol. 3, No. 1, 4–17, Mar. 2015.

[8] Covic, G. A. and J. T. Boys, "Modern trends in inductive power transfer for transportation applications," *IEEE Journal of Emerging and Selected Topics in Power Electronics*, Vol. 1, No. 1, 28–41, Mar. 2013.

[9] Fu, M., H. Yin, M. Liu, and C. Ma, "Loading and power control for a high-efficiency class E PA-driven megahertz WPT system," *IEEE Transactions on Industrial Electronics*, Vol. 63, No. 11, 6867–6876, Nov. 2016.

[10] Aldhaher, S., G. Kkelis, D. C. Yates, and P. D. Mitcheson, "Class EF2 inverters for wireless power transfer applications," in *2015 IEEE Wireless Power Transfer Conference (WPTC)*, 1–4, Boulder, CO, USA, May 2015.

[11] Hui, S. Y. R., W. Zhong, and C. K. Lee, "A critical review of recent progress in mid-range wireless power transfer," *IEEE Transactions on Power Electronics*, Vol. 29, No. 9, 4500–4511, Sep. 2014.

[12] Sohn, Y. H., B. H. Choi, E. S. Lee, G. C. Lim, G.-H. Cho, and C. T. Rim, "General unified analyses of two-capacitor inductive power transfer systems: Equivalence of current-source SS and SP compensations," *IEEE Transactions on Power Electronics*, Vol. 30, No. 11, 6030–6045, Nov. 2015.

[13] Zhang, H., Y. Chen, C.-H. Jo, S.-J. Park, and D.-H. Kim, "Dc-link and switched capacitor control for varying coupling conditions in inductive power transfer system for unmanned aerial vehicles," *IEEE Transactions on Power Electronics*, Vol. 36, No. 5, 5108–5120, May 2021.

[14] Yi, Z., A. Liu, B. Zhou, X.-X. Yang, and M. Li, "A novel interdigital self-resonant coil for inductive power transfer," *IEEE Microwave and Wireless Technology Letters*, Vol. 33, No. 9, 1369–1372, Sep. 2023.

[15] Qin, R. and D. Costinett, "Multi-layer non-uniform series self-resonant coil for wireless power transfer," in *2019 IEEE Energy Conversion Congress and Exposition (ECCE)*, 3333–3339, Baltimore, MD, USA, 2019.

[16] Li, J. and D. Costinett, "Analysis and design of a series self-resonant coil for wireless power transfer," in *2018 IEEE Applied Power Electronics Conference and Exposition (APEC)*, 1052–1059, San Antonio, TX, USA, 2018.

[17] De Miranda, C. M. and S. F. Pichorim, "A self-resonant two-coil wireless power transfer system using open bifilar coils," *IEEE Transactions on Circuits and Systems II: Express Briefs*, Vol. 64, No. 6, 615–619, Jun. 2017.

[18] Kyaw, P. A., A. L. F. Stein, and C. R. Sullivan, "High-Q resonator with integrated capacitance for resonant power conversion," in *2017 IEEE Applied Power Electronics Conference and Exposition (APEC)*, 2519–2526, Tampa, FL, USA, 2017.

[19] Chowdary, K. V. V. S. R., K. Kumar, S. Banerjee, and R. R. Kumar, "Comparative analysis between high-order compensation and ss-compensation for dynamic wireless power transfer system," in *2020 IEEE International Conference on Power Electronics, Drives and Energy Systems (PEDES)*, 1–6, Jaipur, India, Dec. 2020.

[20] Madawala, U. K. and D. J. Thrimawithana, "A bidirectional inductive power interface for electric vehicles in V2G systems," *IEEE Transactions on Industrial Electronics*, Vol. 58, No. 10, 4789–4796, Oct. 2011.

[21] Wang, Y., Z. Sun, Y. Guan, and D. Xu, "Overview of megahertz wireless power transfer," *Proceedings of the IEEE*, Vol. 111, No. 5, 528–554, May 2023.

[22] Liu, M., M. Fu, and C. Ma, "Low-harmonic-contents and high-efficiency class E full-wave current-driven rectifier for megahertz wireless power transfer systems," *IEEE Transactions on Power Electronics*, Vol. 32, No. 2, 1198–1209, Feb. 2017.

[23] Hasani, J. Y. and M. Kamarei, "Analysis and optimum design of a class E RF power amplifier," *IEEE Transactions on Circuits and Systems I: Regular Papers*, Vol. 55, No. 6, 1759–1768, Jul. 2008.

[24] Yi, Z., M. Li, B. Muneer, G. He, and X.-X. Yang, "Self-resonant antisymmetric planar coil for compact inductive power transfer system avoiding compensation circuits," *IEEE Transactions on Power Electronics*, Vol. 36, No. 5, 5121–5134, May 2021.

[25] Suetsugu, T. and M. Kazimierczuk, "Steady-state behavior of class E amplifier outside designed conditions," in *2005 IEEE International Symposium on Circuits and Systems*, Vol. 1, 708–711, Kobe, Japan, 2005.

[26] Yi, Z., M. Li, B. Muneer, and Q. Zhu, "High-efficiency mid-range inductive power transfer employing alternative-winding coils," *IEEE Transactions on Power Electronics*, Vol. 34, No. 7, 6706–6721, Jul. 2019.

[27] Namgoong, G., W. Park, and F. Bien, "A 13.56 MHz wireless power transfer system with fully integrated PLL-based frequency-regulated reconfigurable duty control for implantable medical devices," *IEEE Transactions on Biomedical Circuits and Systems*, Vol. 16, No. 6, 1116–1128, Dec. 2022.

[28] Kim, H., Y. Park, and C. Kim, "A 13.56-MHz wireless power transfer system with a wide operating distance and load range for biometric smartcards," *IEEE Transactions on Power Electronics*, Vol. 38, No. 4, 5576–5585, Apr. 2023.

[29] Bai, X., Y. Lu, C. Zhan, and R. P. Martins, "A 6.78-MHz wireless power transfer system with inherent wireless phase shift control without feedback data sensing coil," *IEEE Journal of Solid-State Circuits*, Vol. 58, No. 6, 1746–1757, Jun. 2023.

[30] Lu, T. and S. Du, "A 13.56 MHz wireless power transfer system with hybrid voltage-/current-mode receiver and global digital-PWM regulation achieving 150% transfer range extension and 72.3% end-to-end efficiency," in *2024 IEEE International Solid-State Circuits Conference (ISSCC)*, Vol. 67, 450–452, San Francisco, CA, USA, Feb. 2024.

[31] De Miranda, C. M. and S. F. Pichorim, "A three-coil wireless power transfer system using self-resonant open-bifilar coils," *AEU — International Journal of Electronics and Communications*, Vol. 154, 154300, 2022.

[32] Yi, Z., K. Yang, X.-X. Yang, M. Li, and D. Zeng, "A gradual-width high-Q self-resonant coil based on coplanar waveguide," *IEEE Microwave and Wireless Technology Letters*, Vol. 35, No. 2, 165–168, Feb. 2025.